Advances in SAR Change Detection

Leslie M. Novak
Scientific Systems Company, Inc.
500 West Cummings Park, Suite 3000
Woburn, MA 01801
UNITED STATES

E-mail: lnovak@ssci.com, novakl@charter.net

ABSTRACT

SAR change detection performance using coherent change detection (CCD) and non-coherent change detection (NCCD) algorithms is demonstrated using high-resolution synthetic aperture radar (SAR) imagery gathered by the General Dynamics Data Collection System. CCD performance comparisons using phase-only imagery versus complex (amplitude and phase) imagery are also presented. A new image quality metric, the "Universal Image Quality Index" is described and used to detect changes between a SAR intensity (reference versus test) image-pair; the change image is shown to be very similar to the corresponding CCD image. Studies of SAR coherent change detection using the Maximum Likelihood Estimate (MLE) of coherence are also presented; detection performance ROCs (PD vs. PFA curves) are presented comparing coherent and non-coherent change detection algorithms (CCD, MLE, and NCCD).

1. INTRODUCTION

Fig.1 shows a typical SAR image gathered by the General Dynamics Data Collection System (DCS). The image size is 4096x4096 pixels and the resolution of the data is 1ft by 1ft. The box superimposed on the image shows a region of interest containing two interesting change detection scenes that will be investigated. These initial non-coherent change detection studies will focus on a scene containing parked vehicles (the "vehicle scene"); the initial coherent change detection studies will focus on a scene containing a subtle man-made disturbance due to people that walked in a grassy area (the "racetrack scene").

Figures 2 and 3 show the 1024x1024 region of interest containing the change detection scenes; Fig.2 is the SAR reference image and Fig.3 is the corresponding SAR test image. These reference and test images will be processed using the coherent change detection (CCD) algorithm [1] and non-coherent change detection (NCCD) algorithm [2] as defined in Table 1.

Table 1: SAR Change Detection algorithms: Coherent Change algorithm (left), Non-Coherent Change algorithm (right).

$$CCD = \frac{\left\lvert \sum_{k=1}^{N} x_k^* x_{k+N} \right\rvert}{\sqrt{\left(\sum_{k=1}^{N} \lvert x_k \rvert^2 \right)\left(\sum_{k=1}^{N} \lvert x_{k+N} \rvert^2 \right)}}$$	$$NCCD = 1 - \frac{\left(\frac{1}{N}\sum_{k=1}^{N} \lvert x_k \rvert^2 \right)\left(\frac{1}{N}\sum_{k=1}^{N} \lvert x_{k+N} \rvert^2 \right)}{\left(\frac{1}{2}\left(\frac{1}{N}\sum_{k=1}^{N} \lvert x_k \rvert^2 + \frac{1}{N}\sum_{k=1}^{N} \lvert x_{k+N} \rvert^2 \right) \right)^2}$$

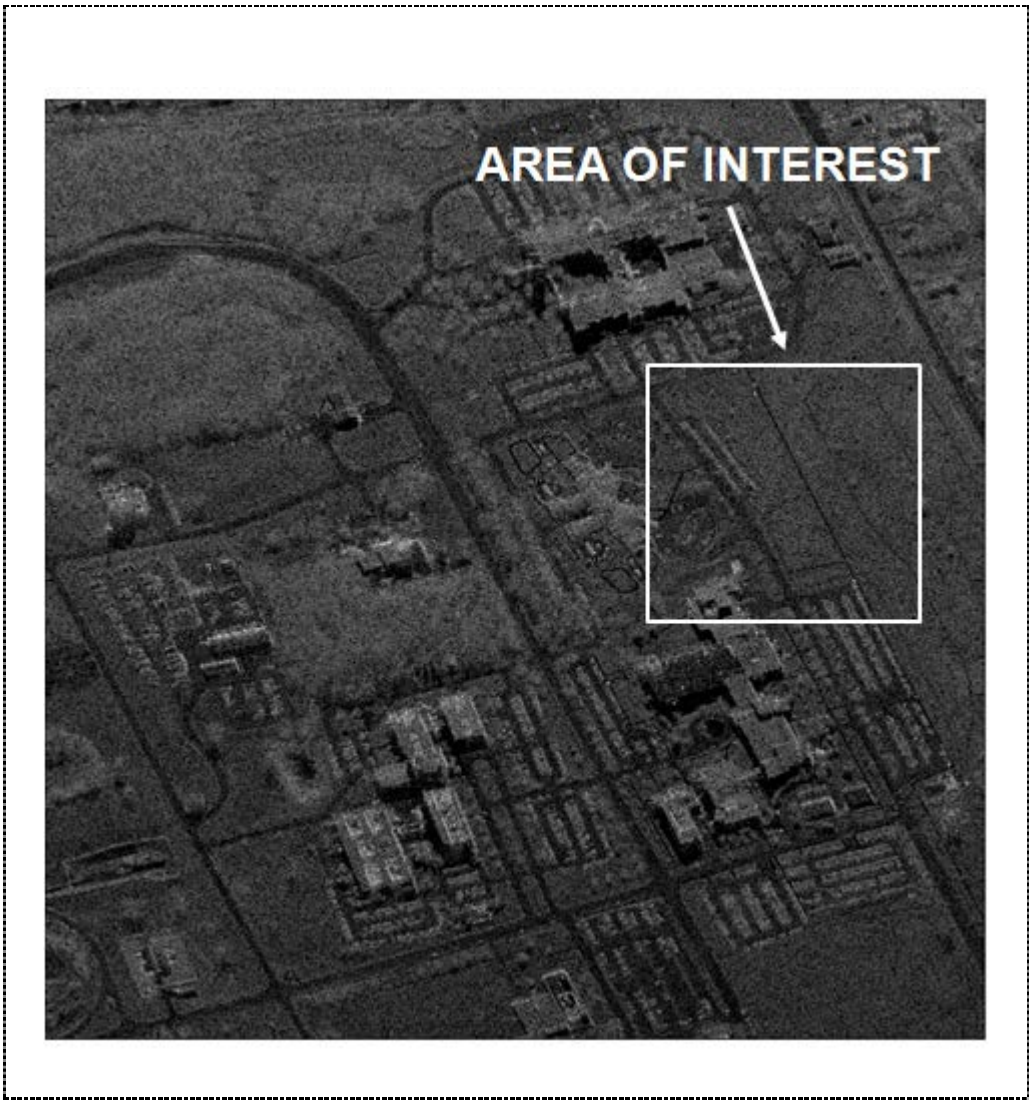

Figure 1: SAR Reference image, size = 4096 x 4096 pixels; area of interest size = 1024 x 1024 pixels.

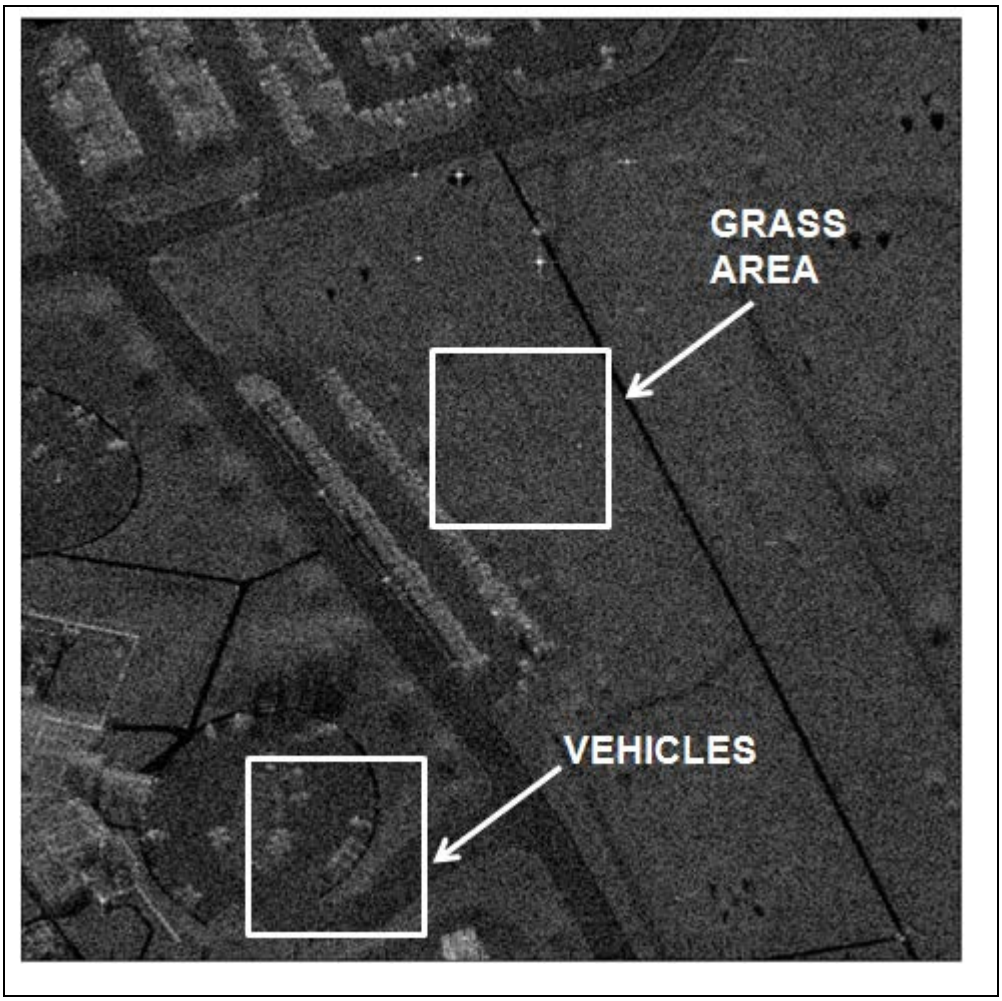

Figure 2: SAR reference image.

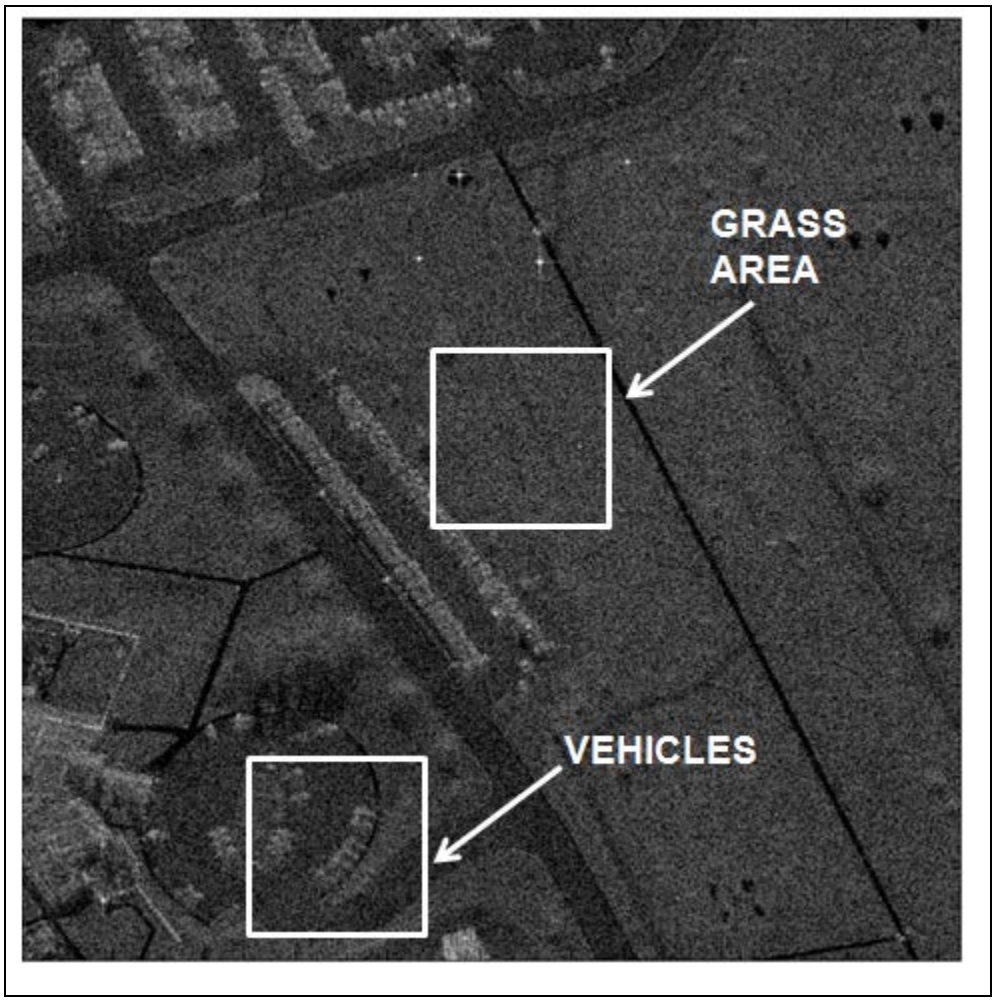

Figure 3: SAR test image.

Figures 4 and 5 show the CCD and NCCD change images obtained from comparisons of a test image and a previously gathered reference image; several detected changes are pointed out on the NCCD and CCD images. Note that only coherent change detection has detected the "racetrack" in the grass area — and although the change in amplitude between the reference and test images is too small to be detected by the NCCD algorithm, the change in phase (i.e., the "coherence") between the reference and test images is sufficient to permit detection of this subtle change by the CCD algorithm.

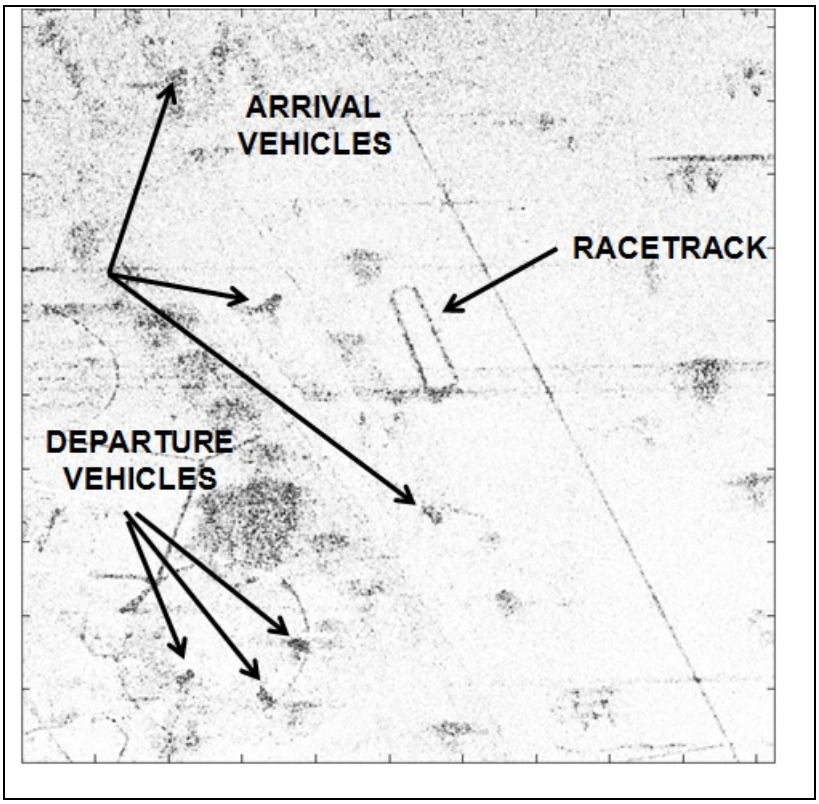

Figure 4: Coherent Change image.

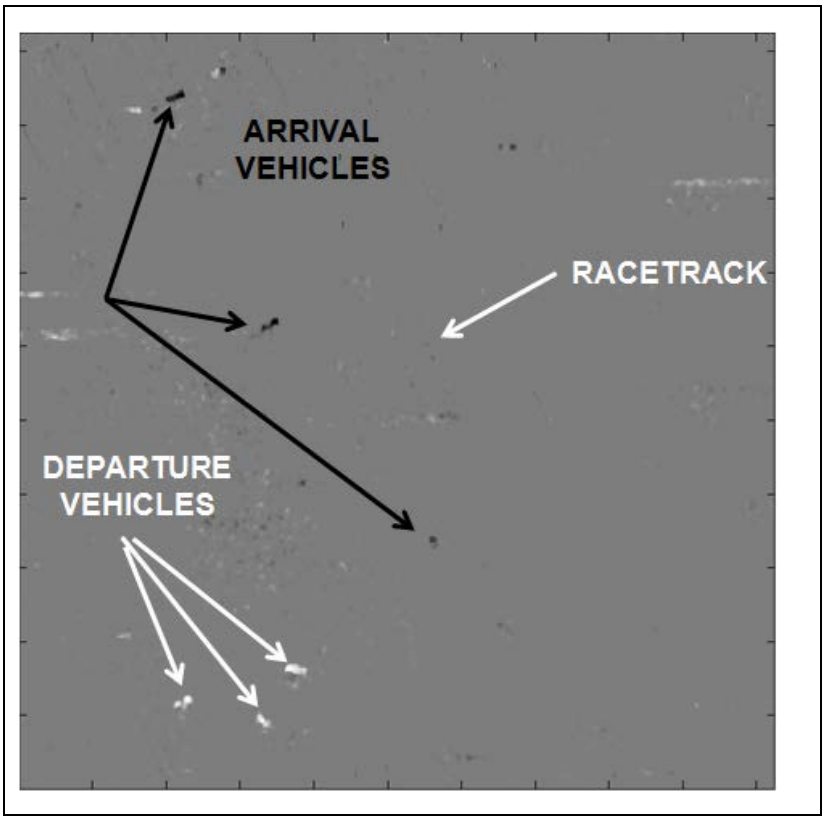

Figure 5: Non-Coherent Change image.

2. AN ANALYSIS OF THE CCD ALGORITHM

Figure 6 presents a simplified block diagram of the baseline coherent change detection (CCD) algorithm we use in these studies. The reference and test images are comprised of complex pixels, denoted as images $X_{m,n}$ and $\vec{X}_{m,n}$. As indicated in the figure, the algorithm calculates the coherence "γ" between the reference and test images (i.e., the magnitude of the complex cross-correlation between the reference and test images). Also in these studies, the coherence is calculated using a 3x3 cluster of the complex image data (thus, M = N = 2).

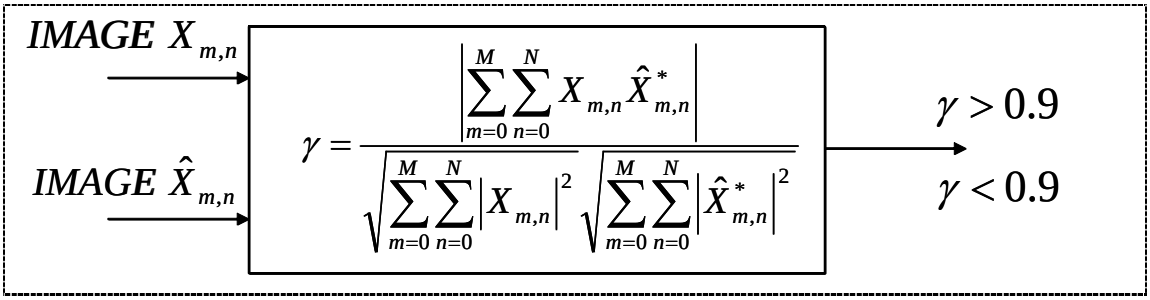

Figure 6: Block diagram of the CCD algorithm.

An analysis of coherent change detection algorithm is given as follows. We write the complex pixel data in amplitude and phase format:

$$X_{m,n} = \left|X_{m,n}\right| e^{j\varphi_{m,n}} \quad and \quad X^{*}_{m,n} = \left|X_{m,n}\right| e^{-j\varphi_{m,n}}$$

The coherence equation defined in Figure 6, expressed in amplitude/phase format, is given as follows:

$$\gamma = \frac{\left|\sum_{m=0}^{M}\sum_{n=o}^{N}\left|X_{m,n}\right|\left|\hat{X}^{*}_{m,n}\right| e^{j(\varphi_{m,n}-\hat{\varphi}_{m,n})}\right|}{\sqrt{\sum_{m=0}^{M}\sum_{n=0}^{N}\left|X_{m,n}\right|^2}\sqrt{\sum_{m=0}^{M}\sum_{n=0}^{N}\left|\hat{X}^{*}_{m,n}\right|^2}}$$

Next we make the assumption that the magnitude of the complex reference and test pixels are equal, implying that the coherence between the images will depend only on the phase differences between pixels. With this simplifying assumption, the following result is obtained:

$$if \ \left|X_{m,n}\right| = \left|\hat{X}_{m,n}\right| = \left|X\right| \ \forall\, m,n \quad then \quad \gamma = \left|\sum_{m=0}^{M}\sum_{n=0}^{N} e^{j(\varphi_{m,n}-\hat{\varphi}_{m,n})}\right|$$

We are interested in comparing the performance of the CCD algorithm using the original complex image data versus using the phase-only data; in this study we initially focus on a sub-image of the grass area including the "racetrack feature". Figure 7 shows a 256x256 pixel coherence image containing the racetrack with a selected patch of grass outlined; note that the average coherence of this 256x256 pixel sub-image is 0.9347.

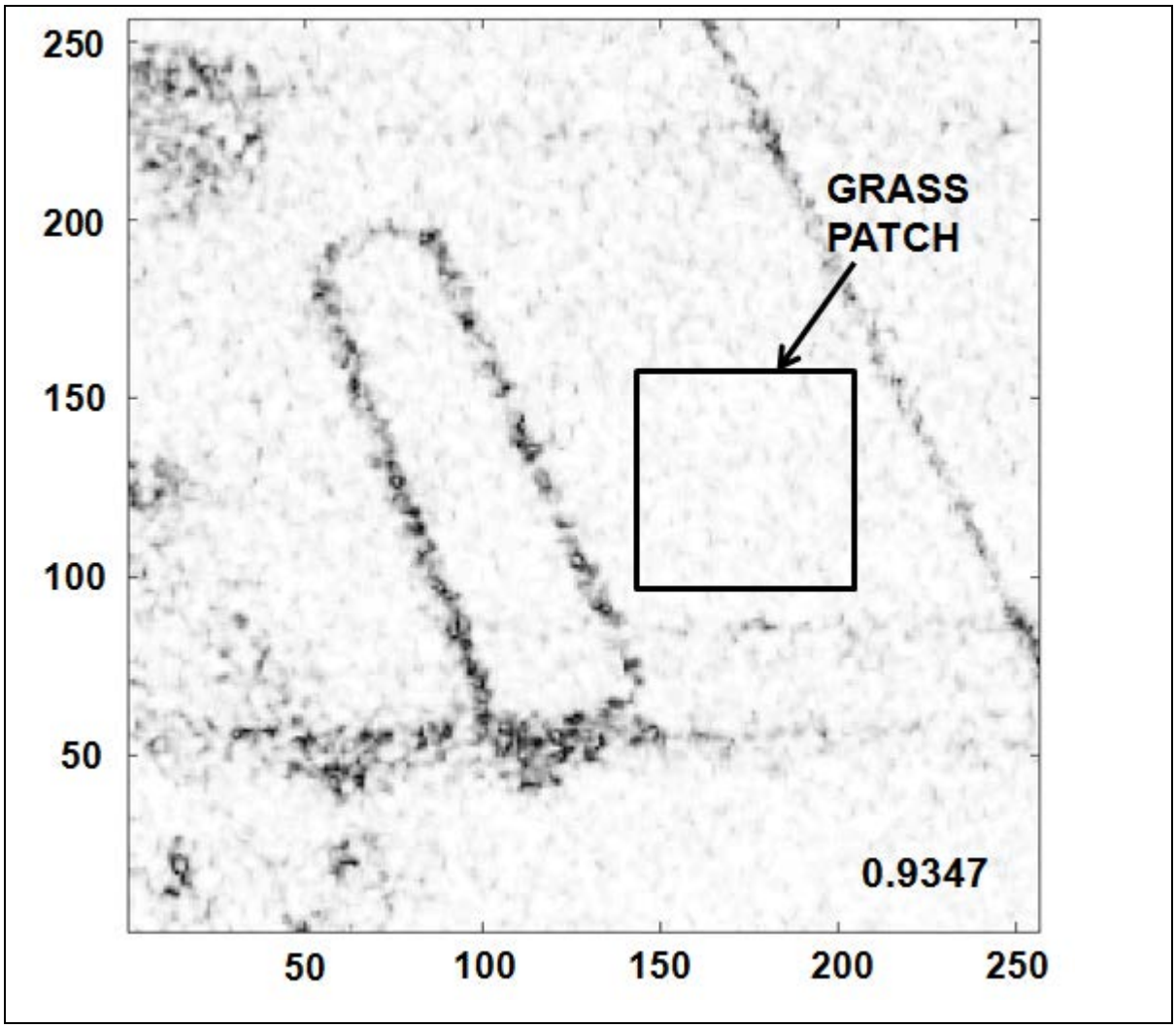

Figure 7: CCD image of "racetrack" area; average image coherence = 0.9347; a grass patch is outlined.

Figures 8 and 9 present a side-by-side comparison of the grass patch CCD images calculated using the original complex SAR data versus using the (amplitude-normalized) phase-only SAR data. This small patch of grass has average coherence = 0.9685 using the original complex SAR data, whereas the average coherence = 0.9361 using phase-only data. Thus, this example seems to indicate that both amplitude and phase (i.e., the complex pixel data) should be used in image exploitation using the CCD algorithm; there appears to be a loss in the level of coherence using phase-only images.

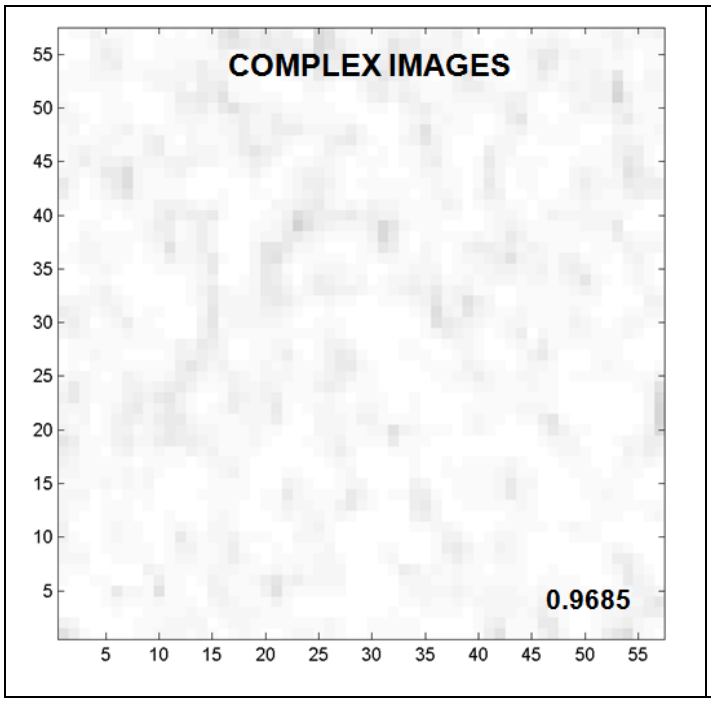

Figure 8: SAR CCD image of grass patch.

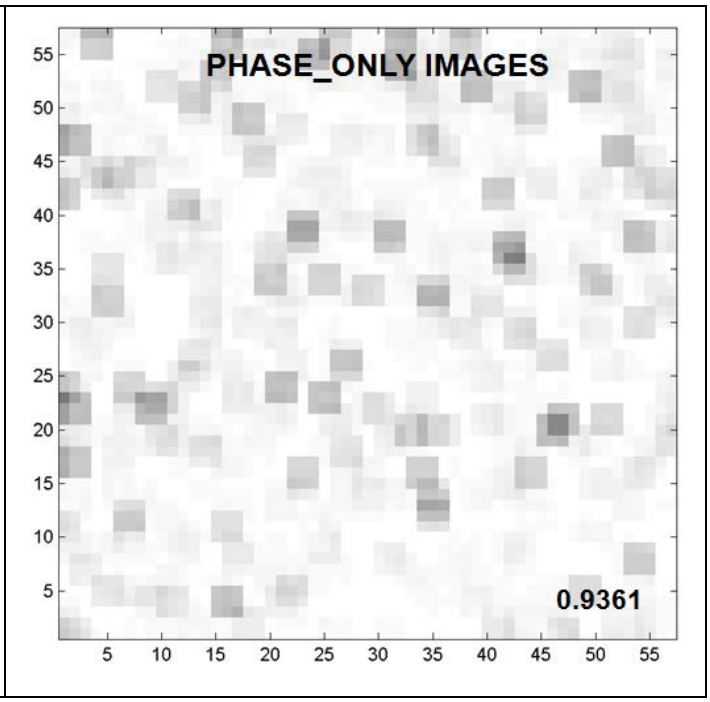

Figure 9: CCD image of grass patch from phase-only images.

Figure 10 validates the conjecture that the best CCD image is obtained using both the amplitude and phase of the data in forming the change image; the figure indicates that the average coherence using complex data which was 0.9347 (see figure 7) has been reduced to 0.8948 using phase-only data -- and the change image in Figure 10 also shows that a larger number of low coherence pixels have been obtained using phase-only data.

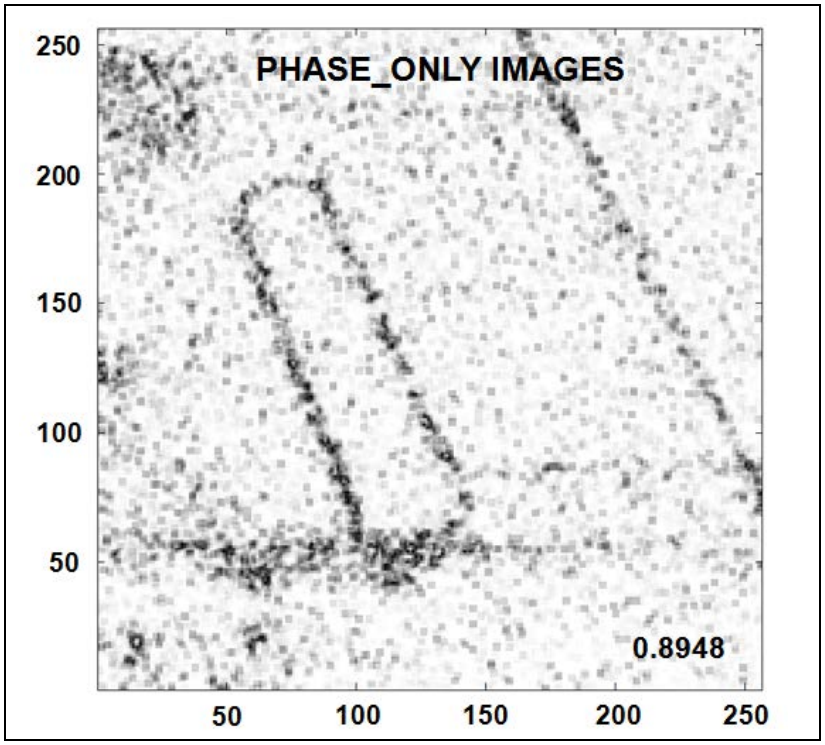

Figure 10: CCD image,"racetrack", phase-only data.

3. RESULTS USING THE "UNIVERSAL IMAGE QUALITY INDEX"

This section presents a summary of some interesting results that were obtained using an approach developed in References 5 and 6; these authors have proposed an image quality metric called the "Universal Image Quality Index" and they have demonstrated the application of their new metric to photographs such as the well-known "Lena" and others. Although our SAR images are comprised of complex pixel values, it was of interest to apply this new metric to SAR intensity images. With this goal in mind, we give a brief description of the new metric and then present results of applying the approach to the SAR imagery shown in the previously described CCD and NCCD studies.

Table 2 presents details of the Universal Image Quality Index. There are two intensity images, denoted as image X and image Y; in the context of SAR change detection, X denotes the reference image (intensity image) and Y denotes the test image (intensity image). The table shows a pair of 3x3 clusters of intensity values to be compared, and our goal is to find the changes between the reference and test intensity images. The mean, variance, and covariance of the intensity values are calculated as indicated in the Table 2.

Table 2: Definition of statistics used in calculating the "universal image quality index".

$image\ X = \begin{pmatrix} x_1 & x_2 & x_3 \\ x_4 & x_5 & x_6 \\ x_7 & x_8 & x_9 \end{pmatrix}$	$image\ Y = \begin{pmatrix} y_1 & y_2 & y_3 \\ y_4 & y_5 & y_6 \\ y_7 & y_8 & y_9 \end{pmatrix}$
$\bar{x} = \frac{1}{N}\sum_{i=1}^{N} x_i$	$\bar{y} = \frac{1}{N}\sum_{i=1}^{N} y_i$
$\sigma_x^2 = \frac{1}{(N-1)}\sum_{i=1}^{N}(x_i - \bar{x})^2$	$\sigma_y^2 = \frac{1}{(N-1)}\sum_{i=1}^{N}(y_i - \bar{y})^2$
$\sigma_{xy} = \frac{1}{(N-1)}\sum_{i=1}^{N}(x_i - \bar{x})(y_i - \bar{y})$	

As presented in Table 3, these mean, variance, and covariance values are used to form three image quality factors: $Q_1, Q_2, and\ Q_3$. Q_1 is a measure of structural similarity, Q_2 is a measure of the similarity of the means, and Q_3 is a measure of the similarity of the contrasts.

Table 3: Definition of the "universal image quality index".

$$Q = \left[\frac{\sigma_{xy}}{\sigma_x \sigma_y}\right]\left[\frac{2\bar{x}\bar{y}}{(\bar{x})^2 + (\bar{y})^2}\right]\left[\frac{2\sigma_x \sigma_y}{\sigma_x^2 + \sigma_y^2}\right] \quad \in [-1,+1]$$

$$Q = Q_1 \times Q_2 \times Q_3$$

$Q_1 = \left[\frac{\sigma_{xy}}{\sigma_x \sigma_y}\right] \in [-1,+1]$	Q_1 : A measure of Image Structural Similarity
$Q_2 = \left[\frac{2\bar{x}\bar{y}}{(\bar{x})^2 + (\bar{y})^2}\right] \in [0,+1]$	Q_2 : Similarity of Image Means
$Q_3 = \left[\frac{2\sigma_x \sigma_y}{\sigma_x^2 + \sigma_y^2}\right] \in [0,+1]$	Q_3 : Similarity of Image Contrasts

The image quality index, Q, is calculated from 3x3 clusters of intensity data at each pixel location in the image, resulting in a new image denoted as the Universal IQ Index Image; this new image is a representation of the changes that exist between the reference and test images. The SAR reference and test images shown previously in Figures 2 and 3 were converted into intensity images and processed as described above. The resulting Universal IQ Index Image we obtained is shown in Figure 11; an average IQ index of 0.8283 was obtained from the image shown. The interesting observation gleaned from the image shown in Figure 11 is that this change image visually appears to be a CCD image – but this change image was obtained from intensity-only SAR reference and test imagery.

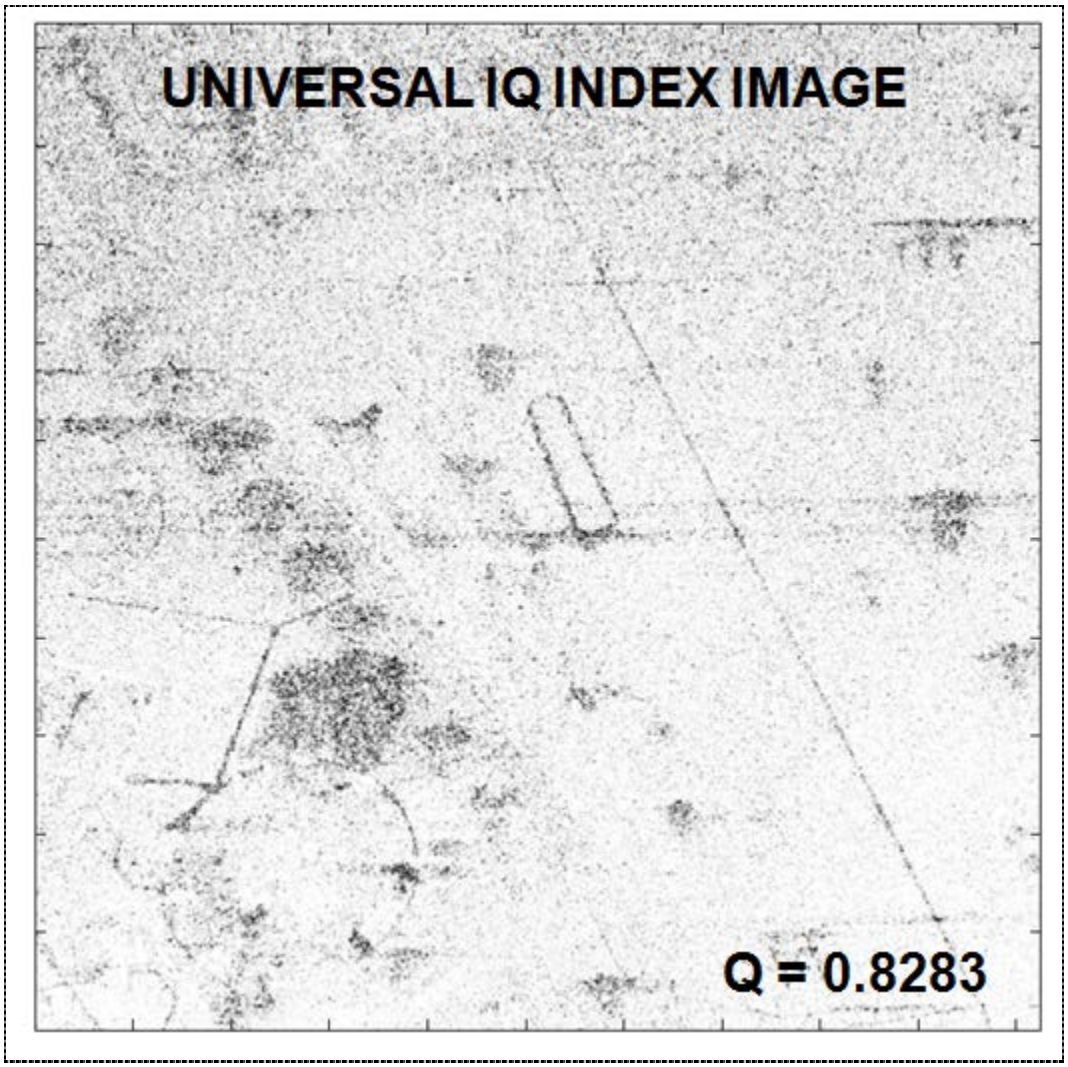

Figure 11: Universal image quality index image obtained using intensity images shown in figures 2 & 3.

Further analysis of the images produced by each of the factors $Q_1, Q_2, and\ Q_3$ showed that the image produced by the factor Q_1 was the dominant image, and this factor is simply the cross-correlation of the SAR intensity images. This observation has resulted in our researching the literature on previous mathematical analyses of the cross-correlation of SAR intensity images and its relationship with the SAR coherence parameter (see References 7 and 8). Table 4 presents two functional relationships derived in the references. ρ_A corresponds to intensity cross-correlation without mean removal (Reference 7) and ρ_B corresponds to intensity cross-correlation with mean removal (Reference 8).

Table 4: Coherence relations vs. cross-correlation of SAR intensity images.

Intensity Correlation	Coherence Relationship
ρ_A	$\gamma_A = \sqrt{2\rho_A - 1}\,; \quad \rho_A \geq 0.5$ $\gamma_A = 0\,; \quad \rho_A < 0.5$
ρ_B	$\gamma_B = \sqrt{\rho_B}\,; \quad 0 < \rho_B \leq 1.0$

Additional SAR change detection studies using the intensity cross-correlation denoted as ρ_B in Table 3 were performed. Figure 12 presents a side-by-side comparison of the Coherence Image (left) versus the corresponding change image obtained using the intensity image cross-correlation denoted as ρ_B in Table 4. Visually these images look quite similar -- and the absolute value of the difference between these images is presented in Figure 13. The difference error image shows reasonably small differences between the actual coherence values, γ, and the coherence estimates $\gamma_B = \sqrt{\rho_B}$.

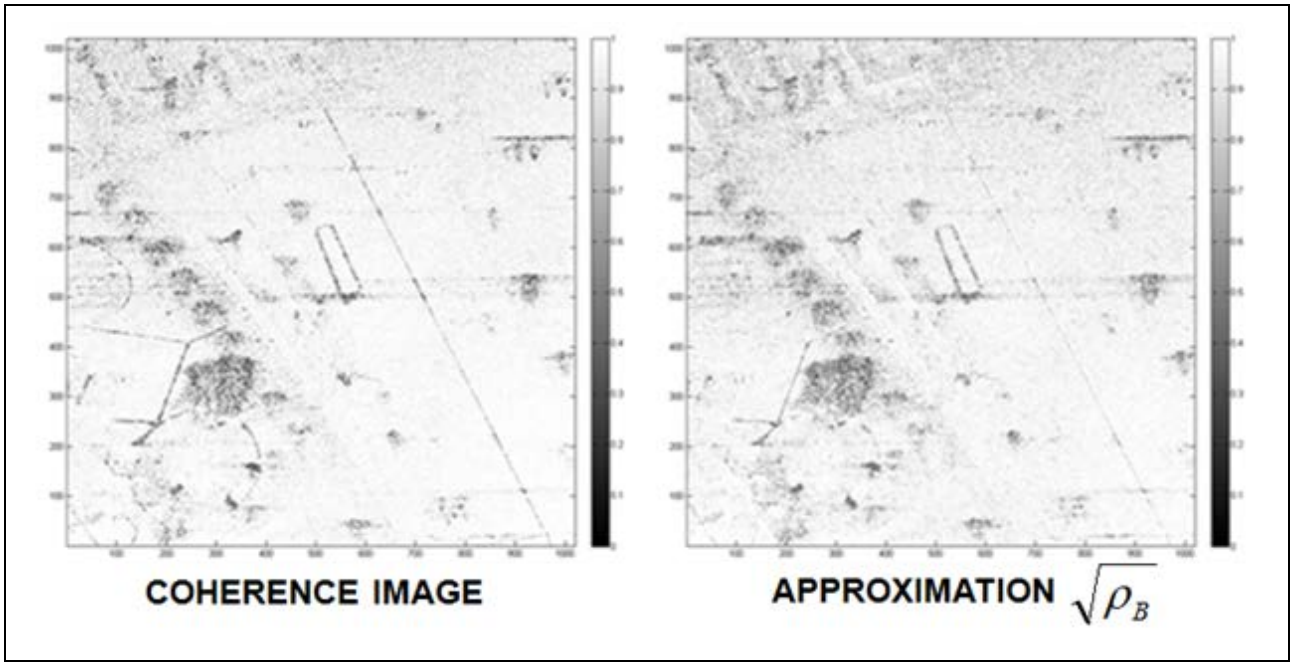

Figure 12: Coherence image vs. approximation.

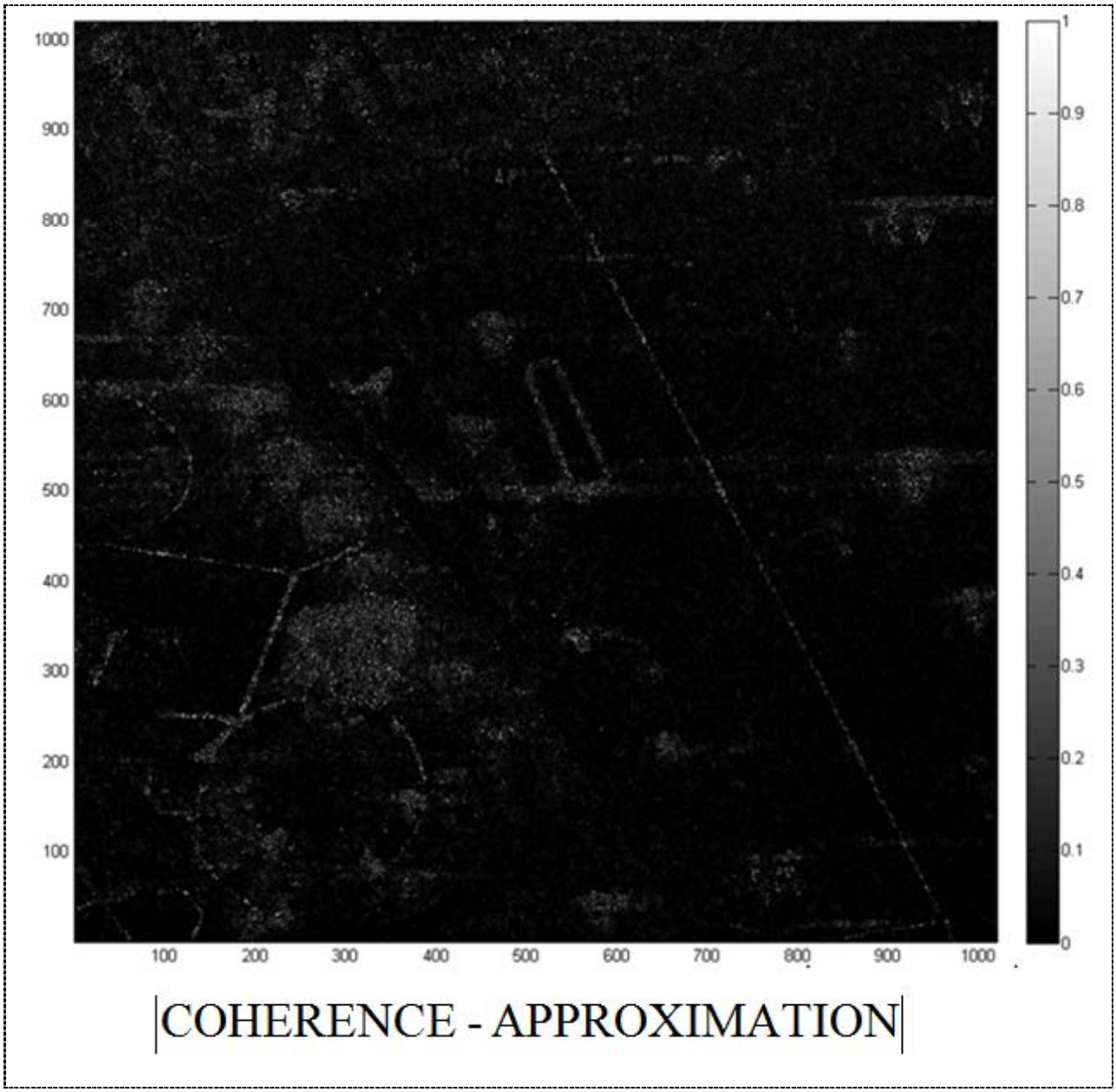

Figure 13: Magnitude of difference image.

4. PERFORMANCE COMPARISON OF CHANGE DETECTION ALGORITHMS

In the previous sections we presented some preliminary comparisons of the CCD vs. NCCD change detection algorithms. In this section we will investigate the detection performance of the Maximum Likelihood Estimate (MLE) of the SAR coherence parameter. We will quantify and compare the change detection performance of the MLE versus the CCD. In Table 5 below we present the definitions of these SAR coherent change detection algorithms. We will also compare the detection performance of these coherent change detection algorithms with the baseline non-coherent change detection (NCCD) algorithm defined previously in Table 1.

In our previous change detection studies we found that the MLE version of the coherent change detection algorithm gave better detection performance results than the (complex cross-correlation) CCD version of the algorithm. These previously obtained results were in agreement with a paper presented by Miriam Cha of MIT Lincoln Laboratory at the IEEE Statistical Signal Processing Workshop, Ann Arbor, Michigan (Reference [9]). In Miriam Cha's paper, it was conjectured, based on theoretical analyses of the MLE and CCD coherent change detection algorithms, that the MLE version should provide better coherent change detection performance (i.e., PD vs. PFA ROCs) than the CCD version if the reference and test images have approximately equal underlying variances. Clearly, this is the case for the accurately calibrated SAR imagery used in our studies [10]. In this section we summarize our studies of these two coherent change detection algorithms. Our goal is to determine the sensitivity of the MLE algorithm when the test image variance is not comparable to the reference image variance. We aim to show that the MLE outperforms the CCD over some range of calibration gain offsets between the reference and test images, thus, we aim to verify the conjecture of Miriam Cha.

Table 5: Coherent change algorithms

$$CCD = \frac{\left\lvert \sum_{k=1}^{N} x_k^* x_{k+N} \right\rvert}{\sqrt{\left(\sum_{k=1}^{N} \lvert x_k \rvert^2 \right)\left(\sum_{k=1}^{N} \lvert x_{k+N} \rvert^2 \right)}}$$
$$MLE = \frac{\left\lvert \sum_{k=1}^{N} x_k^* x_{k+N} \right\rvert}{\frac{1}{2}\left(\sum_{k=1}^{N} \lvert x_k \rvert^2 + \sum_{k=1}^{N} \lvert x_{k+N} \rvert^2 \right)}$$

Figure 14 shows an aerial photo of the "Area-of-Interest" selected for our SAR change detection studies. The area of interest is comprised of several parking lots which are occupied by numerous parked (i.e., stationary) vehicles. Analysis of the SAR reference and test images of this area were found to contain a total of 33 vehicles that changed during the time interval between the gathering of the reference and test images. This set of 33 vehicles were either "arrivals" or departures" that occurred during the time interval between the gathering of the reference and test images.

Figure 14: Aerial photograph of the "area of interest" selected for CCD studies.

Figure 15 presents the SAR reference and test images used in this change detection study. The locations of the change-detected vehicles are shown as circles superimposed on the images. There are a total of 33 vehicle detections in these SAR images; both arrivals and departures are contained in the 33 circles. These change detections were verified by visually flickering between the reference and test SAR images.

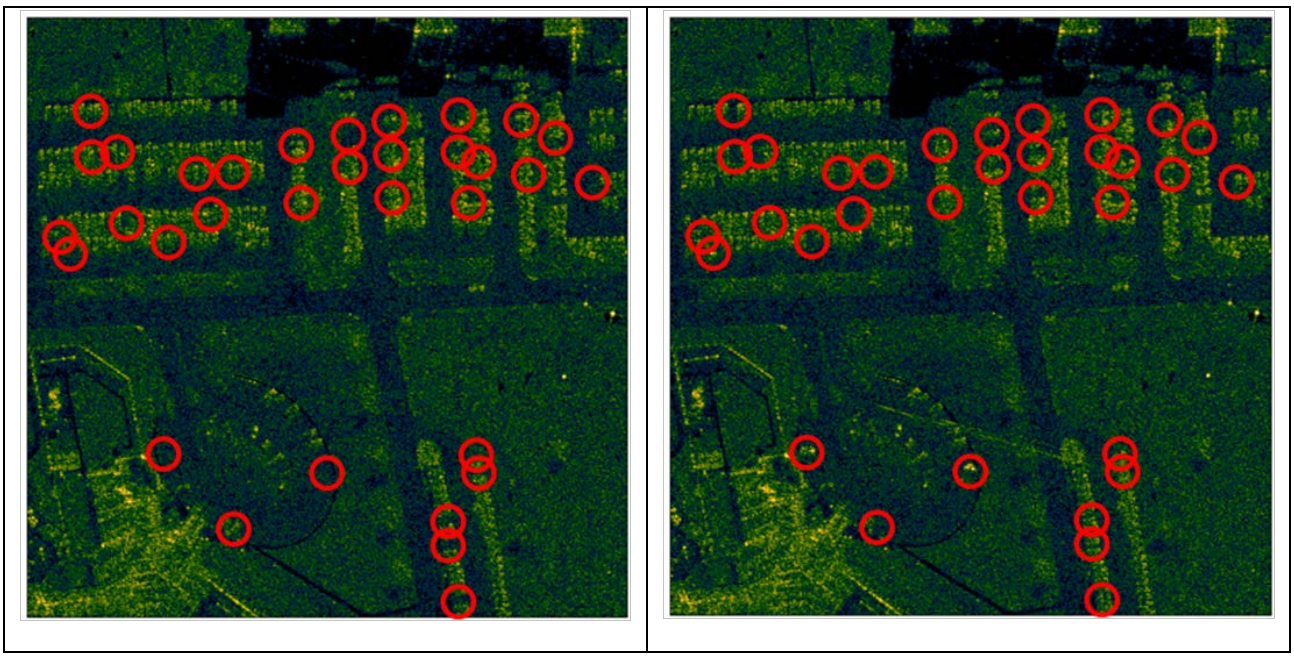

Figure 15: SAR reference image (left), SAR test image (right).

Figure 16 (left) shows a binary image of the locations of the change-detected vehicles. This binary image is used as ground truth for the targets in these CCD/MLE/NCCD change detection studies. We use the ground truth image to score the performance of the coherent and non-coherent change detection algorithms evaluated in the studies. Detections that occur in the black areas are scored as target detections. Detections that occur in the white background area are scored as false alarms. In Figure 16 (right) we show a "don't care" band constructed around each of the targets to prevent clutter false alarms from being declared targets.

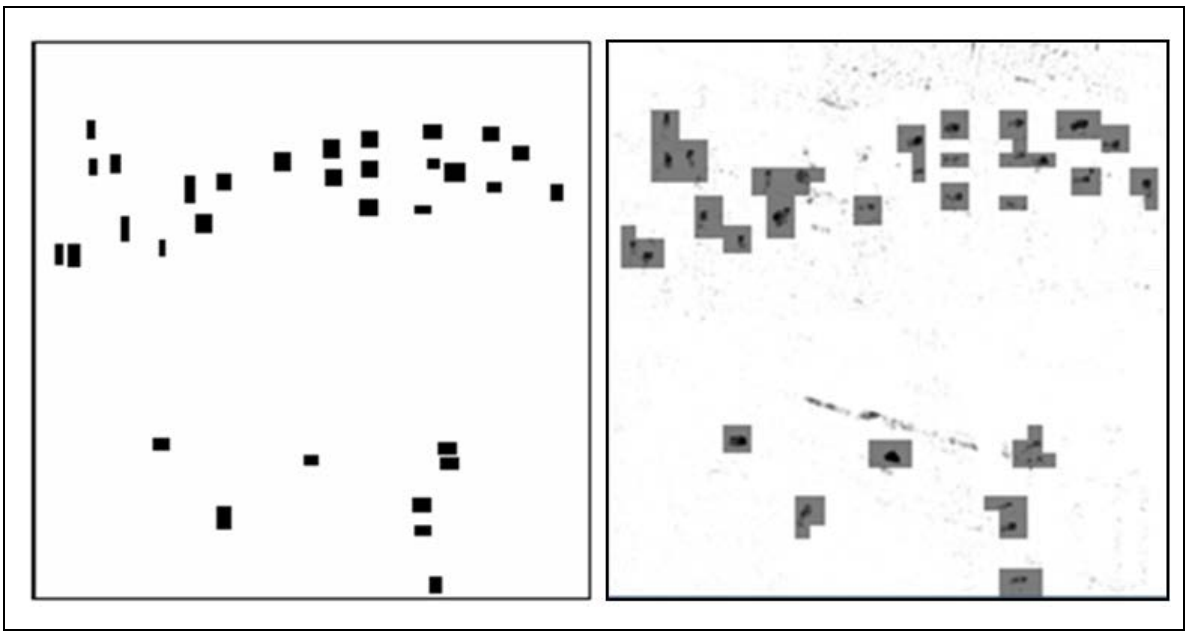

Figure 16: Locations of CD targets (left); masked locations of CD targets (right).

Table 5 above gives mathematical equations defining the SAR change detection algorithms to be evaluated and compared in these studies. Two versions of the coherent change detection algorithm are given -- these are denoted as MLE and CCD, depending on the algorithm normalization used. Note that the MLE normalizes the numerator by a sum of the reference and test pixel powers, whereas the CCD normalizes the numerator by a product of the reference and test powers. The CCD algorithm is the well-known complex cross-correlation algorithm used for calculating (estimating) the coherence between complex-valued reference and test images; we refer to this algorithm as the "CCD". Since the MLE algorithm is actually the Maximum Likelihood Estimate of the coherence parameter, we refer to this algorithm as the "MLE". The non-coherent SAR change detection algorithm evaluated in these studies was given above in Table 1; we refer to this algorithm as the "NCCD".

A comparison of the performance of these SAR change detection algorithms is given in the following Figures 17-20; these figures show PD versus PFA obtained via change detection processing using CD-algorithm box sizes 3x3, 5x5, 7x7, and 9x9, respectively. Figure 17 shows the PD/PFA ROC curves obtained using a 3x3 CD-algorithm box size; the curves show that coherent change detection using the MLE algorithm achieves significantly better detection performance than the classical CCD algorithm. At 70% PD, CCD gave ≈ 700 target-sized FAs, whereas the MLE gave ≈ 0 FAs. We also observe that the non-coherent NCCD change detection provides better performance than both of the coherent change detection algorithms. We evaluated detection performance versus the percentage (%) of detected pixels in a target-sixe box, and we found that detection performance was not very sensitive to this parameter; the ROC curves obtained for 5% to 30% are tightly clustered.

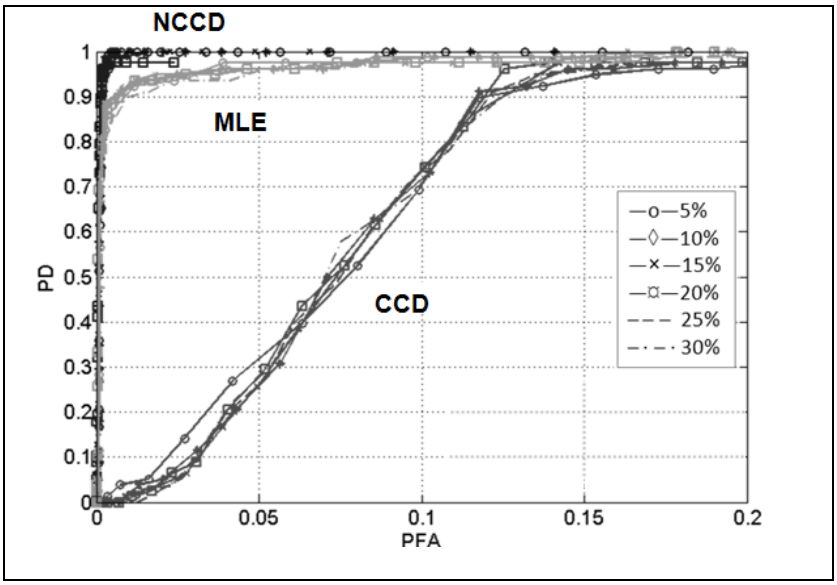

Figure 17: Change detection performance ROCs; CD algorithm box size = 3x3.

Figure 18 summarizes change detection performance using a CD algorithm box size of 5x5. The ROCs shown are similar to those shown in the previous Figure 17. Figure 18 shows that NCCD performance is definitely improved using the larger 5x5 box size – and CCD performance is also improved with the larger box size. The MLE algorithm shows slightly degraded performance with the larger box size.

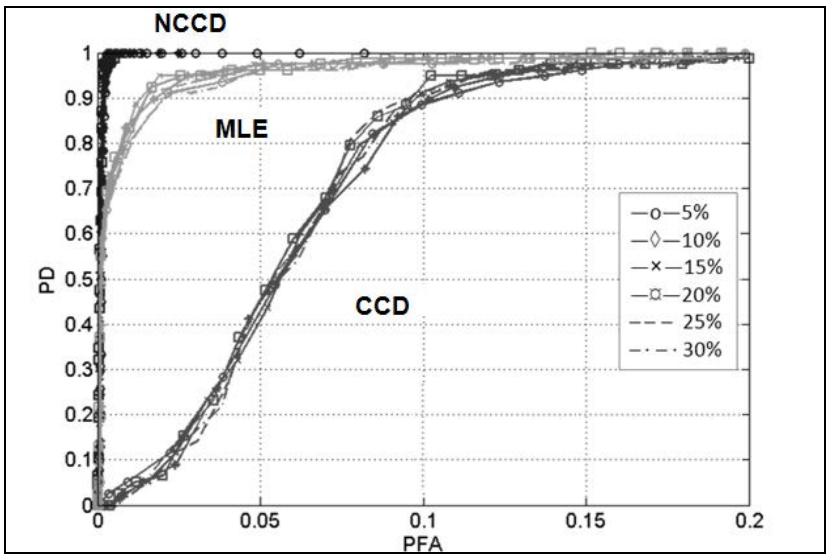

Figure 18: Change detection performance ROCs; CD algorithm box size = 5x5.

Figure 19 summarizes CCD, MLE and NCCD algorithm performance using a CD algorithm box size of 7x7 to construct the change images. The ROCs shown are similar to those shown in the previous figures. NCCD performance is again somewhat improved using a larger (7x7) box size. The CCD performance is also improved with the larger box size; for example, PD > 90% is achieved with PFA ≈ 0.1 (approximately 700 FAs). The MLE algorithm has better ROC performance than the classical CCD algorithm, but again NCCD gave the best performance.

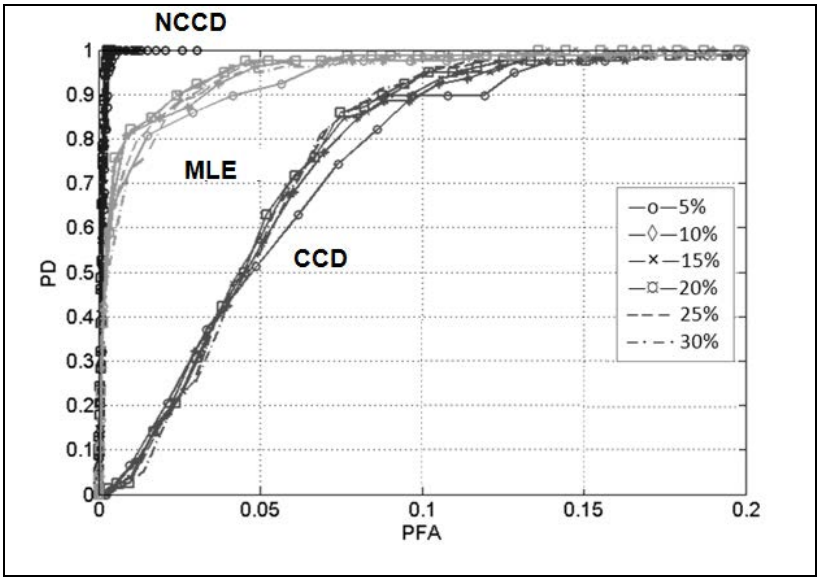

Figure 19: Change detection performance ROCs; CD algorithm box size = 7x7.

Figure 20 summarizes CCD, MLE and NCCD performance using a 9x9 box size. Coherent change detection using the MLE provides significantly better detection performance than the classical CCD algorithm. At 60% PD, the CCD gave approximately "350" target-sized FAs, whereas MLE gave many fewer FAs. Again we observe that the NCCD algorithm gave better performance than both coherent change detection algorithms.

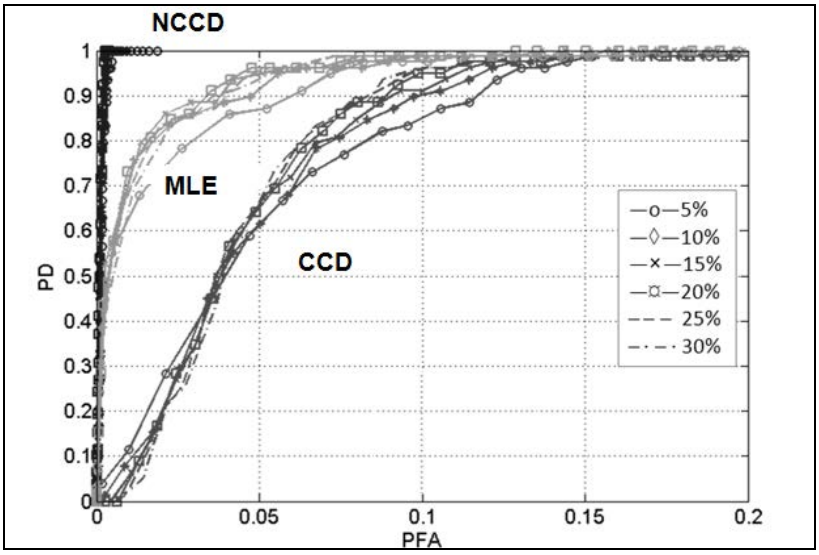

Figure 20: Change detection performance ROCs; CD algorithm box size = 9x9.

In this paragraph we briefly summarize the findings of our change detection algorithm comparison studies described above. For the target and clutter data used in our studies, we found that the non-coherent change detection (NCCD) algorithm achieved the best overall detection performance; this was true for all box-sizes tested, and larger box-sizes gave marginally improved ROCs. PD/PFA curves were not very sensitive to the detector "Fill" parameter from 5% to 30%. The MLE version of the coherent change detector gave better detection performance than the CCD version of the algorithm, and the smaller box size (3x3) gave the best MLE performance.

4.1 Visual Comparisons of the MLE and CCD Algorithms

In this section we will evaluate and visually compare change images from the CCD and MLE versions of the coherent change algorithm with the test image scaled in amplitude relative to the given reference image. In these initial studies we scaled the test image by 0 dB, +3 dB and +6 dB relative to the original reference image. Figure 21 compares CCD and MLE change images obtained using the Gotcha SAR reference and test images (with K = 1, i.e., no test image gain offset). Using Gotcha SAR imagery [10] similar to that used in our studies, MIT Lincoln Laboratory also showed that an MLE change image has higher contrast than the corresponding CCD change image; this phenomenon was demonstrated via change images similar to those shown in Figure 21. Note that the average coherence values of the MLE and CCD change images shown in Figure 21 are 0.8747 vs. 0.9007, respectively; nevertheless, we show that the change vehicles in the MLE image are more easily detected than the change vehicles in the CCD image.

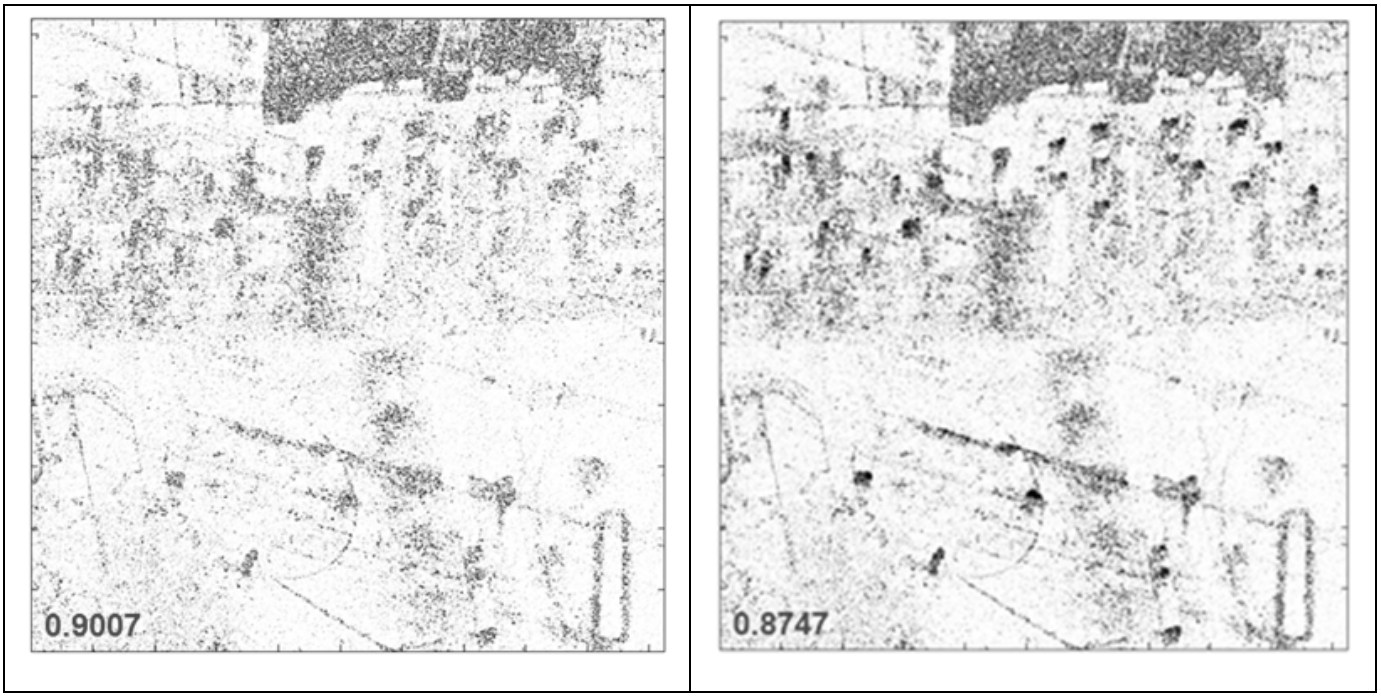

Figure 21: Baseline performance; left, CCD image; right, MLE image.

Figure 22 shows additional examples of MLE change images obtained using amplitude scaled test images; these change images were obtained by comparing the reference image with a scaled test image, (K*(test image)), where the scale factor, K, was either sqrt(2), or 2. The MLE baseline (K = 1) average coherence of 0.8747 has been reduced from this value to 0.8316 and 0.7163 for gain offsets of +3 dB and +6 dB, respectively. Although these change images have less average coherence, it remains to be determined what these test image gain offsets will do to the detectability of the change vehicles in these images.

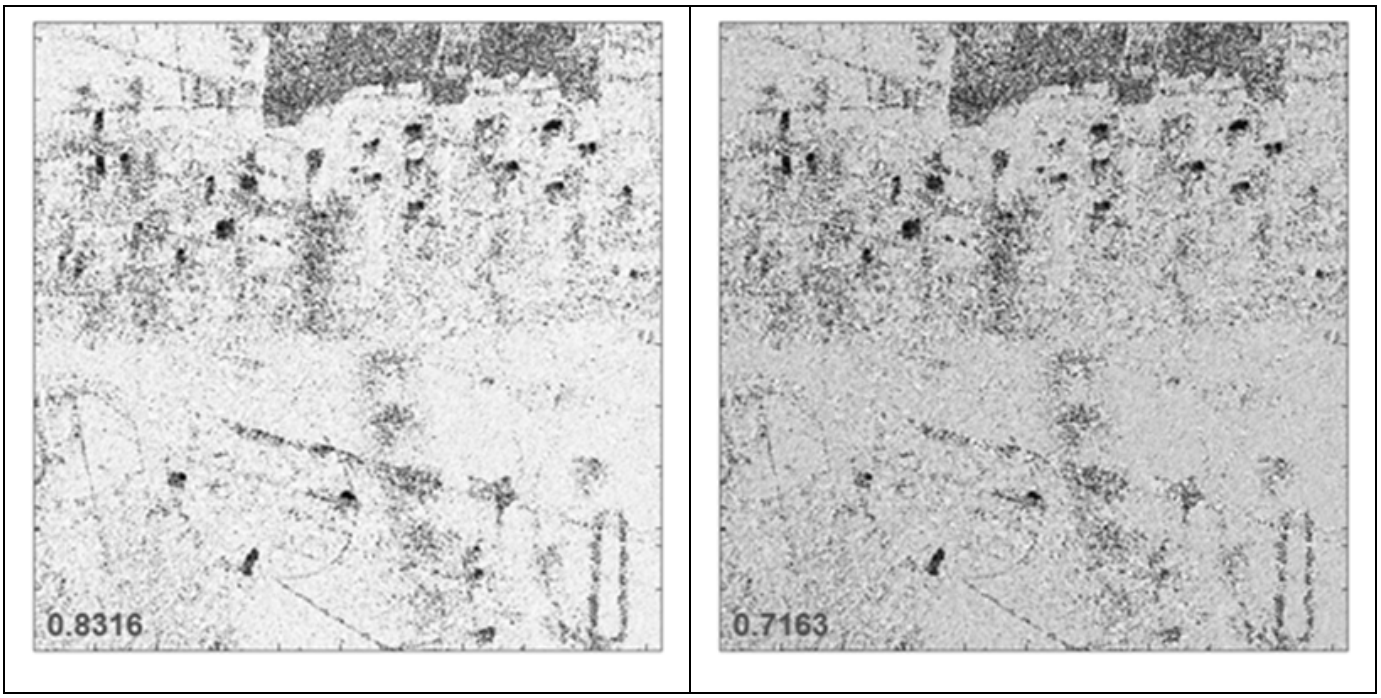

Figure 22: Left, MLE image, K = sqrt (2); right, MLE image, K = 2.

We continued these studies in order to quantify the actual change detection performance (PD vs. PFA) achieved as a function of the test image gain offset parameter, K. First we determined the average coherence values obtained from the CCD and MLE algorithms versus the test image gain offset for offsets as large as 10dB; Figure 23 presents these results. The data given in that figure indicates that the CCD algorithm is unaffected by the gain imbalance, whereas the average coherence estimated from the MLE algorithm is reduced in magnitude as the gain imbalance is increased. Thus, the PD/PFA ROC curves obtained using the CCD version of the coherent change algorithm will be unaffected by the gain offset, and the corresponding change images for the CCD algorithm will be identical to the left image in Figure 21.

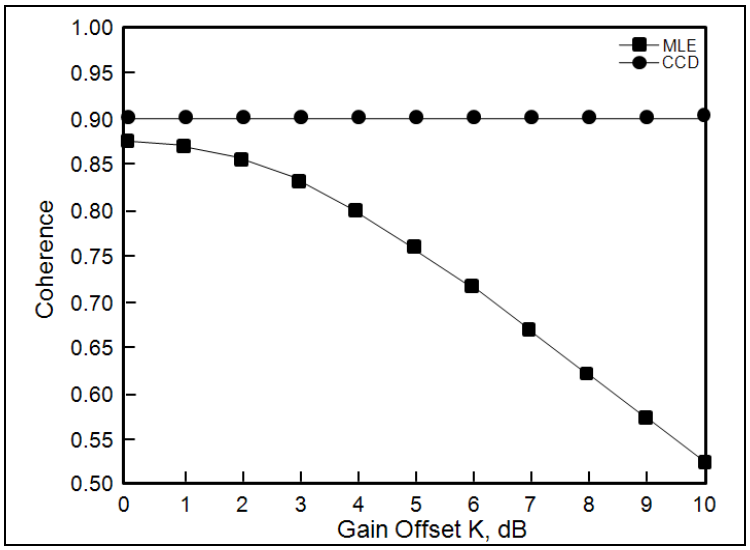

Figure 23: Average change image coherence vs. test image gain offset K in dB.

We evaluated the change detection performance ROCs for this range of gain offsets – these ROCs are shown in Figure 24. The curves in Figure 24 show that MLE change detection performance is superior to CCD change detection performance for PFA < 0.04 -- this is true over the range of gain offsets simulated. It is of interest to visually compare the false alarms and missed targets when an identical number of targets are detected by each algorithm. To this end, we have selected detection thresholds for the CCD and MLE algorithms, resulting in an identical number of targets detected (see operating points at PD = 0.82 in Figure 24). The corresponding PFA values at these operating points are 0.05 vs. 0.014 for the CCD and MLE algorithms, respectively. The MLE PD/PFA curve used in this comparison is the 3 dB gain offset case.

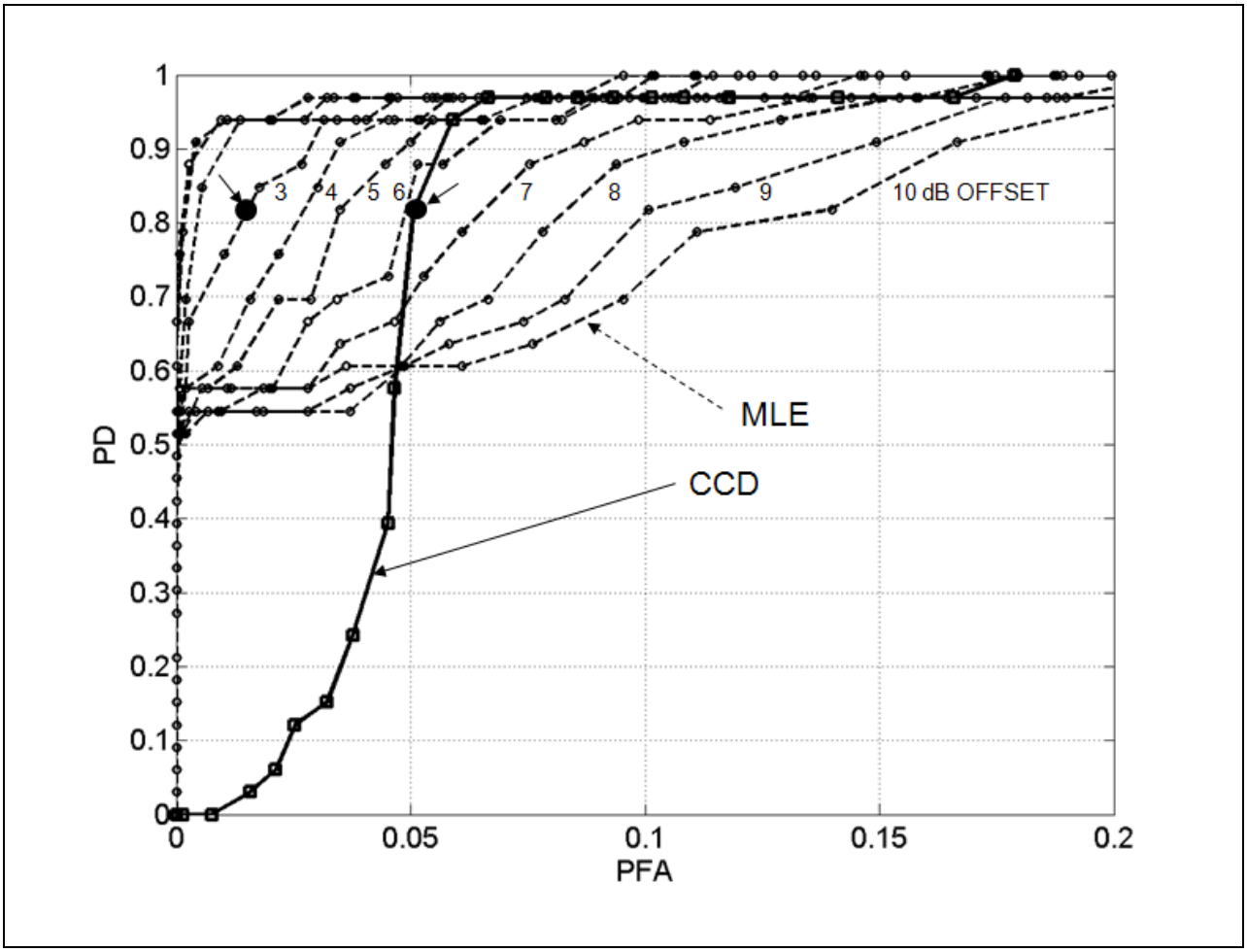

Figure 24: Coherent change detection ROCs for baseline CCD vs. MLE; note the CCD & MLE (3dB) operating points at pd = 0.82.

Figure 25 below shows the CCD change image at the selected operating point. The detection threshold used to obtain PD = 0.82 was 0.488. In this figure, detected targets are overlaid with Circles, false detections are overlaid with Squares, and missed targets are overlaid with Diamonds. At PD = 0.82 there are 6 missed targets (Diamonds) and 73 false detections (Squares). Note that there are a total of 64 false detections in the shadow region below the large building, whereas there are only 9 false detections in the remaining areas of the image. In the next section we will consider the problem of mitigating false detections in SAR image shadow regions – and we will present a simple, robust algorithm for performing this task.

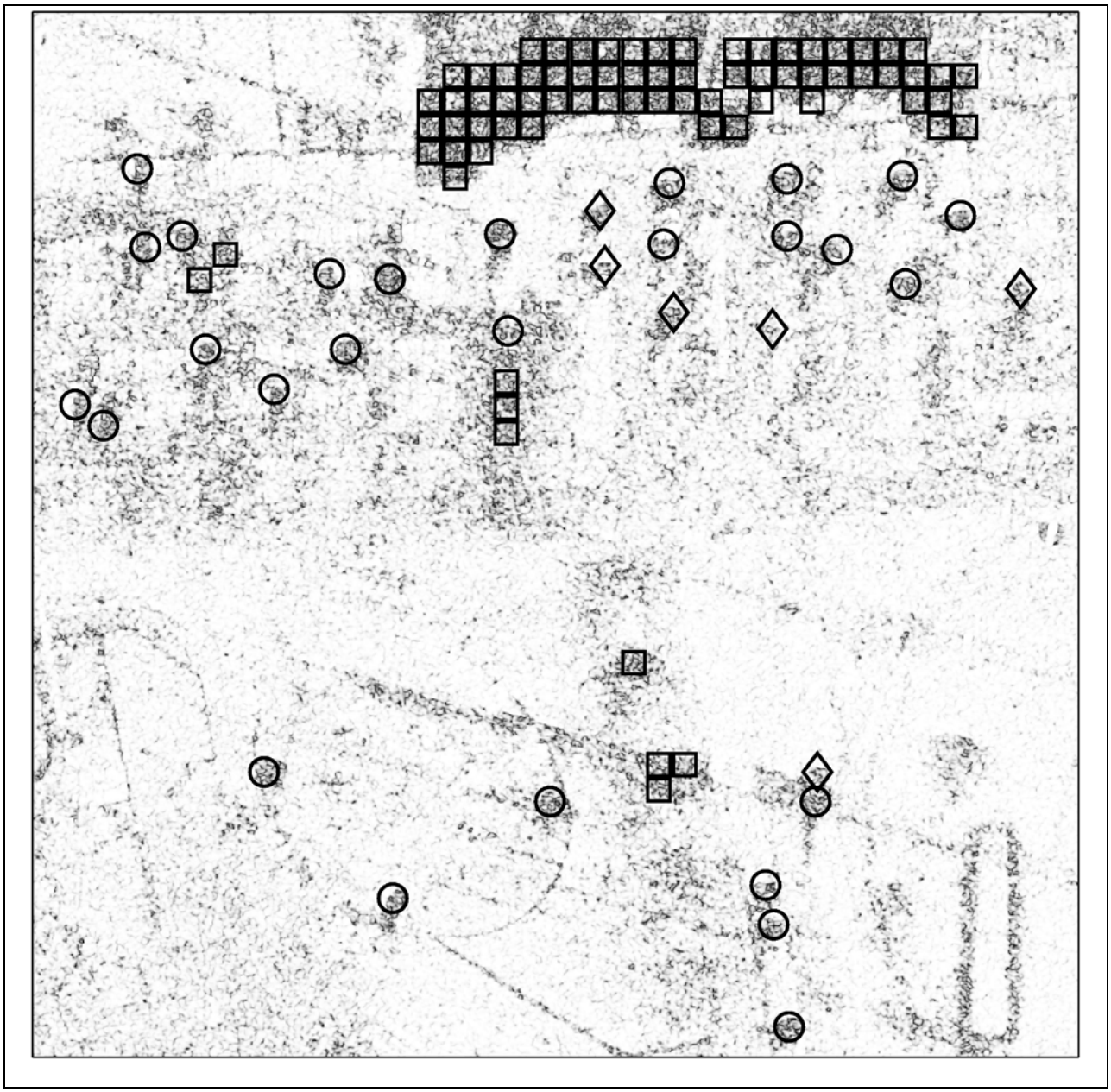

Figure 25: CCD change image, PD = 0.82, PFA = 0.05, missed targets = 6; threshold = 0.488, detection fill percentage = 15%.

Figure 26 shows the corresponding MLE change image at the selected PD = 0.82 operating point. For this change image the detection threshold used to obtain PD = 0.82 is 0.273. Note that the detection overlays on the images illustrate that a different set of targets were missed by the CD algorithms, and hence, each algorithm detects a somewhat different set of the targets. It is also important to point out that although both algorithms obtain false detections in the shadow regions below the large building, the CCD version of the algorithm obtains many more false detections in these shadow regions. In the next section we will develop and evaluate the performance of a simple approach to locate the shadow regions (tree and building shadows) and remove false detections from the SAR change image. Our algorithm for mitigating false detections in these shadow regions will, of course, improve the performance of both algorithms.

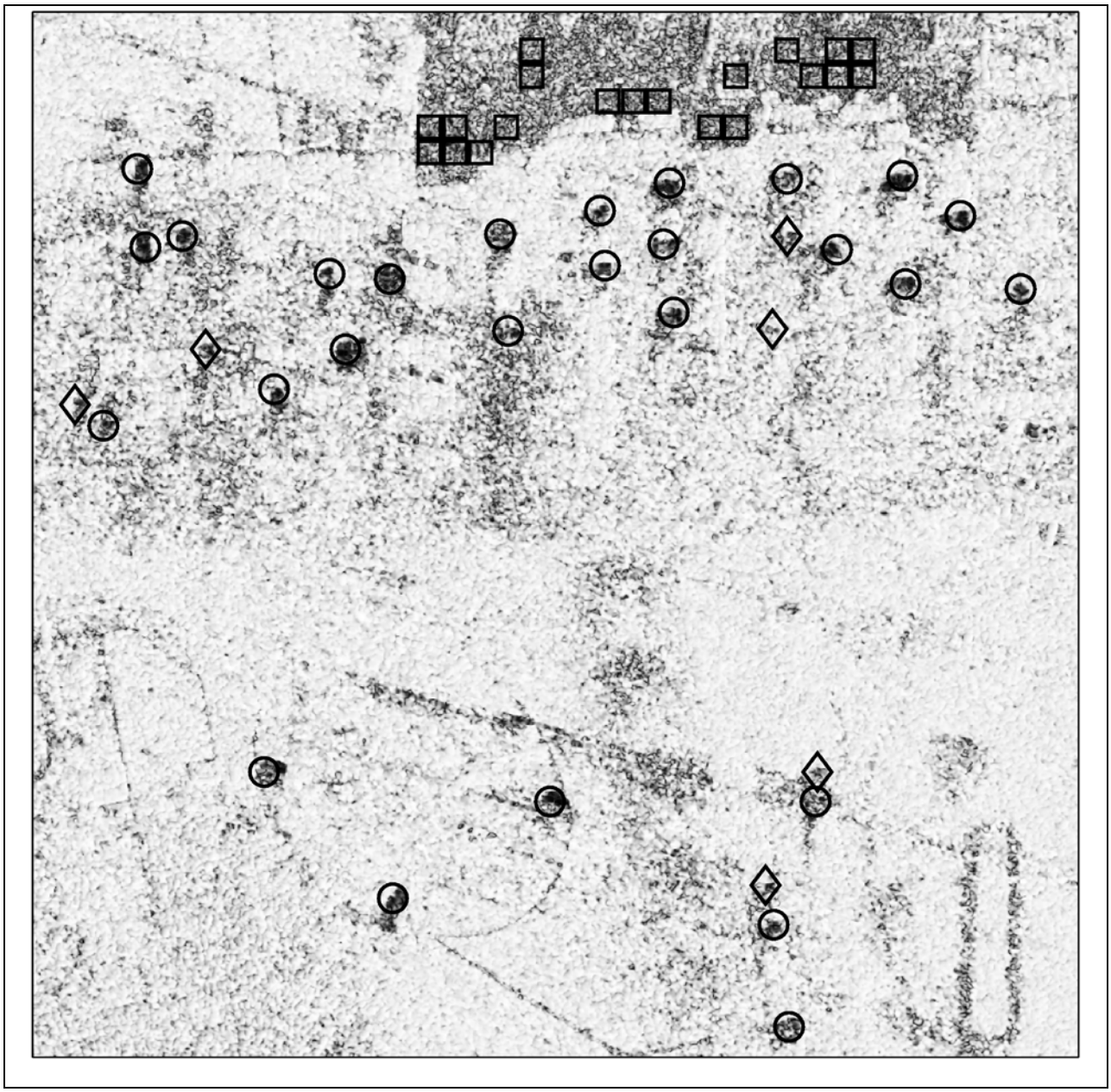

Figure 26: MLE change image, PD = 0.82, PFA = 0.014, missed targets = 6; threshold = 0.273, detection fill percentage = 15%.

Table 6 presents a detection performance comparison of the CCD and MLE algorithms before and after the building shadow false alarms are excluded from the false alarm (FA) calculation. This comparison shows that a significant improvement in coherent change detection performance could be achieved by mitigating false detections in shadow regions of SAR change imagery.

Table 6: Coherent Change Detection statistics, MLE vs. CCD at PD = 0.8182.

	With Building FAs		Without Building FAs	
	PD	# FAs	PD	# FAs
MLE	27/33	20	27/33	0
CCD	27/33	73	27/33	9

4.2 Coherent Change Detection Performance with Shadow Regions Masked

The Maximum Likelihood Estimate (MLE) of the SAR coherence parameter was derived by Charles Jackowatz in Reference [1]. In the previous subsection we showed that using the MLE algorithm to estimate SAR change image coherence could give better target detection performance than using the complex correlation coefficient, CCD. Furthermore, in figures 25 & 26 we observed that many false detections can occur in low-coherence building (and tree) shadows. Low-RCS areas such as building shadows and tree shadows, as well as flat asphalt roads have low coherence due to random phase returns. Since an X-band SAR can't detect target returns from targets located and masked in shadow areas, then CCD performance ROCs could be significantly improved if such areas were masked as "don't care" areas before performing the detection operation.

One simple approach for improving the ROC curves is to post-process the standard CCD and MLE images by setting the coherence of the areas that correspond to low-RCS areas in both the test and reference images to unity. Target detection is then performed on the change images with low RCS areas masked. The low RCS areas can easily be detected as follows. The *n*-th pixel in the CCD image is declared as belonging to the non-interesting, low RCS area if the average power of the coherent sum and the coherent difference between the corresponding neighborhoods in the test and reference images is below a selected threshold, T :

$$\frac{1}{2}\left(\frac{1}{N}\sum_{k\in\Delta_n}|f_k+g_k|^2+\frac{1}{N}\sum_{k\in\Delta_n}|f_k-g_k|^2\right)<T$$

where N is the number of pixels in the local neighborhood, Δ_n, of the *n*-th pixel. f_k and g_k are the *k*-th pixel of the reference and test data in the *n*-th pixel neighborhood, Δ_n.

This subsection applies the above algorithm for detecting low-RCS areas in the SAR scene and removing false detections from these regions of the scene. The gain in detection performance achieved will be quantified via ROC curves. We first show the SAR reference and test images used in these studies (Figures 27 and 28). We also show the ground truth overlay and the low-RCS mask (figures 29 and 30).

Figure 27: SAR reference image.

Figure 28: SAR test image.

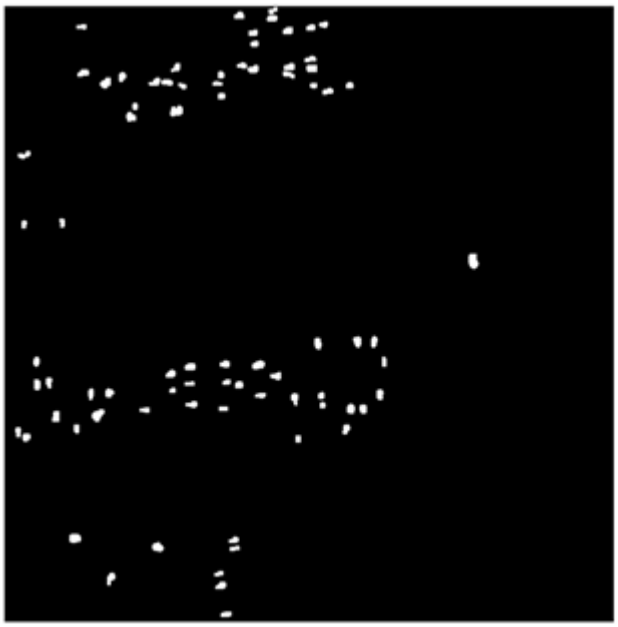

Figure 29: Ground truth overlay.

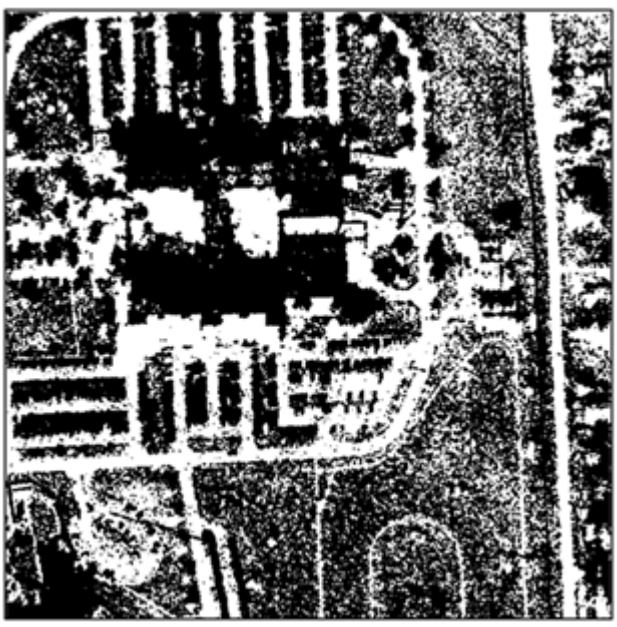

Figure 30: Example low-RCS image.

Coherent change detection performance was determined using the ground truth overlay shown above in Figure 29. Figure 31 shows the original baseline (K = 1)MLE change image and Figure 32 shows the MLE image after applying shadow removal using the low-RCS image shown in Figure 30. Note that after shadow removal, the average MLE change image coherence has increased from 0.8325 to 0.9108.

Figure 31: MLE, no shadow removal.

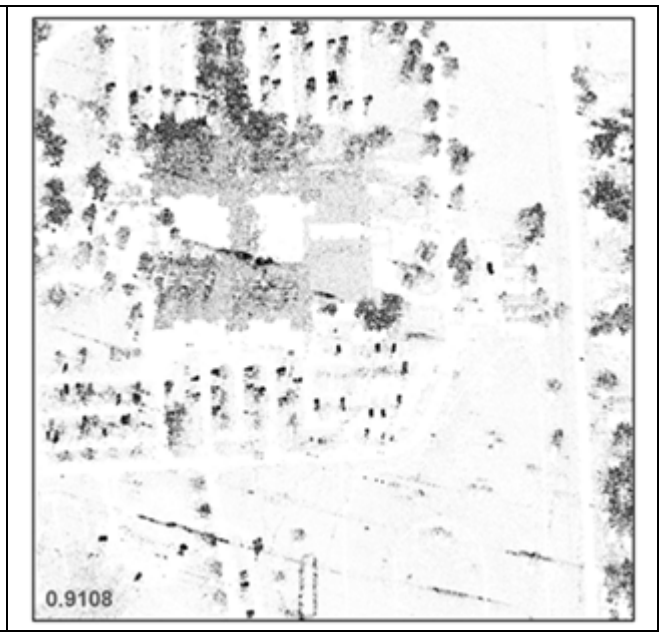

Figure 32: MLE, after shadow removal.

The ROC curves in Figure 33 show that a large gain in coherent change detection performance is achieved after the shadow areas in the SAR image are detected and denoted as "don't care" areas of the scene. From the curves we see that after shadow removal, CCD performance is significantly improved relative to the original CCD performance; however, the CCD algorithm performance after shadow removal is not as good as the original MLE performance – and MLE performance after shadow removal is the best overall change detection performance result.

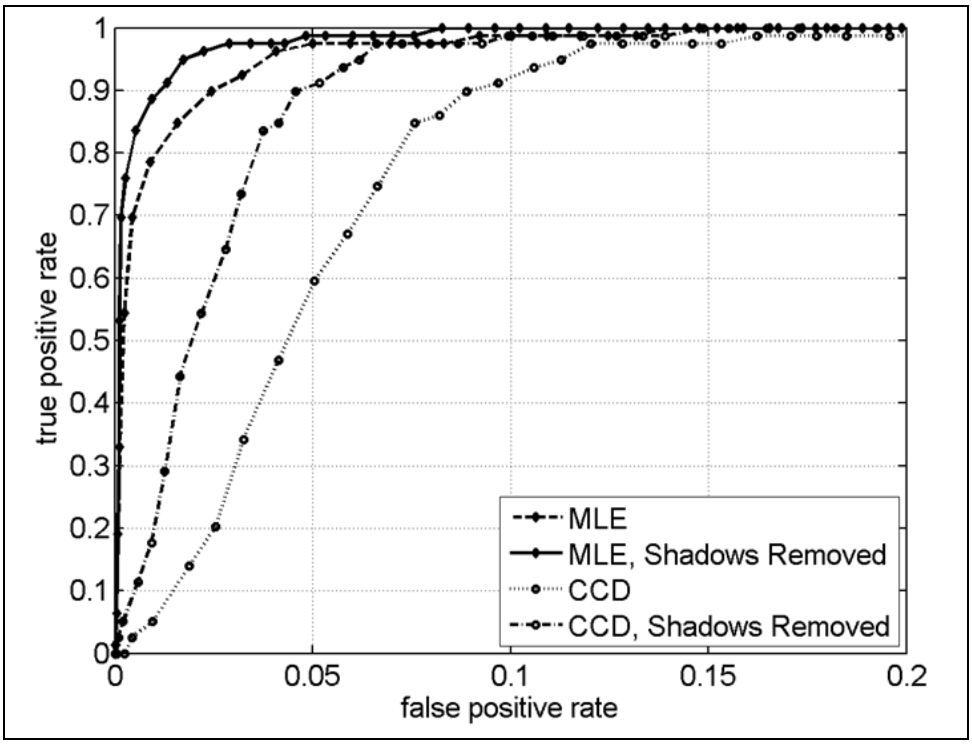

Figure 33: Coherent Change Detection ROCs (true positive rate vs. false positive rate).

5. SUMMARY AND CONCLUSIONS

This paper reviewed some of the basic properties of SAR change detection. An example was presented comparing CCD and NCCD performance using a scene containing various types of changes that occurred between the SAR reference image and test image pair. Another example was presented comparing CCD performance using phase-only SAR images versus using the complex (amplitude and phase) SAR images -- for the images used in this study we found that the coherence levels obtained from the complex imagery were somewhat better than the coherence levels obtained from the phase-only imagery.

A new image quality metric [5, 6], the "Universal Image Quality Index" was investigated. Applying this image quality metric to SAR intensity images (reference versus test intensity images) we observed that the Universal IQ Image was visually quite similar to the SAR CCD coherence image. We then investigated the relationship between the coherence calculated using complex image data and the correlation calculated using the corresponding intensity images. We demonstrated that the magnitude of the differences between the actual coherence image and the estimated coherence image obtained from the intensity-derived correlation image were quite small, however, further analysis is needed to quantify the errors versus the registration accuracy required between reference and test images.

We also compared the coherent change detection performance obtained using the maximum likelihood estimate of the coherence between the reference and test complex SAR images versus using the complex correlation coefficient estimate. We showed, using an example change detection image pair from the publically released Gotcha SAR imagery [10], that the MLE algorithm gave better PD/PFA detection ROCs than the CCD algorithm. Finally, we presented a simple, robust algorithm for mitigation of false changes in shadow areas (building and tree shadows), thereby improving the performance of both coherent change detection algorithms (MLE and CCD).

6. REFERENCES

[1] Jackowatz, C., et al.,"Spotlight-Mode Synthetic Aperture Radar: A Signal Processing Approach," Springer New York, pp. 330-340, 1996.

[2] Preiss, M. and N. Stacy, "Coherent Change Detection: Theoretical Description and Experimental Results," Intelligence, Surveillance and Reconnaissance Division, Defense Science and Technology Organisation, DSTO–TR–1851.

[3] Novak, L., "Coherent Change Detection for Multi-polarization SAR," Asilomar Conference on Circuits, Systems, and Computers, Pacific Grove, CA, October, 2005.

[4] Novak, L., "Change Detection for Multi-polarization, Multi-pass SAR," SPIE Conference on Algorithms for Synthetic Aperture Radar Imagery, Orlando, FL, March, 2005.

[5] Wang, Z. and A. Bovic, "A Universal Image Quality Index," IEEE Signal Processing Letters, March 2002.

[6] Wang, Z. and A. Bovic, "Mean Squared Error: Love It or Leave It," IEEE Signal Processing Magazine, January 2009.

[7] Guarnieri, A. and C. Prati, "SAR Interferometry: A "Quick and Dirty" Coherence Estimator for Data Browsing," IEEE Trans. G.R.S., May 1997

[8] R.Touzi, et al, "Coherence Estimation for SAR Imagery," IEEE Trans. G.R.S., Jan.1999.

[9] Cha, M,. et al, "Test Statistics for Synthetic Aperture Radar Coherent Change Detection," IEEE Statistical Signal Processing Workshop, Ann Arbor, Michigan, 5-8 August, 2012.

[10] Scarborough, S., et al., "A Challenge Problem for SAR Change Detection and Data Compression," SPIE Conference on Algorithms for Synthetic Aperture Radar Imagery, Orlando, FL, April, 2010.